Site-Directed Spin-Labeling Study of the Light-Harvesting Complex CP29

Aleh A. Kavalenka,[†‡] Ruud B. Spruijt,[†] Cor J. A. M. Wolfs,[†] Janez Štrancar,[‡] Roberta Croce,[§] Marcus A. Hemminga,[†*] and Herbert van Amerongen[†]

[†]Laboratory of Biophysics, Wageningen University, Dreijenlaan 3, NL-6703HA Wageningen, The Netherlands; [‡]Jožef Stefan Institute, Jamova 39, SI-1000 Ljubljana, Slovenia; [§]Department of Biophysical Chemistry/Groningen Biomolecular Sciences and Biotechnology Institute, University of Groningen, Nijenborgh 4, NL-9747 AG Groningen, The Netherlands

ABSTRACT The topology of the long N-terminal domain (~100 amino-acid residues) of the photosynthetic Lhc CP29 was studied using electron spin resonance. Wild-type protein containing a single cysteine at position 108 and nine single-cysteine mutants were produced, allowing to label different parts of the domain with a nitroxide spin label. In all cases, the apoproteins were either solubilized in detergent or they were reconstituted with their native pigments (holoproteins) in vitro. The spin-label electron spin resonance spectra were analyzed in terms of a multicomponent spectral simulation approach, based on hybrid evolutionary optimization and solution condensation. These results permit to trace the structural organization of the long N-terminal domain of CP29. Amino-acid residues 97 and 108 are located in the transmembrane pigment-containing protein body of the protein. Positions 65, 81, and 90 are located in a flexible loop that is proposed to extend out of the protein from the stromal surface. This loop also contains a phosphorylation site at Thr81, suggesting that the flexibility of this loop might play a role in the regulatory mechanisms of the light-harvesting process. Positions 4, 33, 40, and 56 are found to be located in a relatively rigid environment, close to the transmembrane protein body. On the other hand, position 15 is located in a flexible region, relatively far away from the transmembrane domain.

INTRODUCTION

Photosynthesis in green plants and algae occurs in chloroplasts. Their highly folded thylakoid membranes provide a home for the multisubunit protein complexes PSI and PSII, which work in concert (linked by a cytochrome b6f complex) to convert sunlight energy into chemical energy (1). The fourth major player is the ATP-synthase complex that uses the proton gradient across the thylakoid membrane, created by PSI/PSII, to convert ADP into ATP. PSI and PSII are supramolecular complexes composed of a core moiety, which contains all the cofactors of the electron transport chain and of an outer antenna system, the role of which is to collect light energy and transfer it to the reaction center where it can be used to drive charge separation. All antenna complexes of higher plants belong to the Lhc multigenic family (2). In particular, six different gene products (Lhcb1–6) compose the outer antenna system of PSII. The major antenna complex of PSII is LHCII, the product of the genes Lhcb1–3 (3), harboring over 50% of the pigments, and it is organized as trimers at the periphery of the PSII supramolecular complex (4). Three minor antenna complexes, CP29 (Lhcb4), CP26 (Lhcb5), and CP24 (Lhcb6) are located in between the LHCII trimers and the core complex, and they are present as monomers. Recently, it has been proposed that the minor antenna complexes provide the sites of nonphotochemical quenching, a mechanism that protects PSII against photoinhibition (5). In particular it has been shown that in CP29, a radical cation is formed on the zeaxanthin in the L2 site, which strongly interacts with Chl A5 (6), leading to the harmless dissipation of excess excitation energy.

The structure of LHCII has been resolved at 2.72 Å (7) showing three transmembrane helices, two amphipathic helices on the lumenal side of the membrane, and the positions of 14 Chl and 4 xanthophyll molecules per monomeric subunit. Structural information on the minor antenna complexes CP24, CP26, and CP29 is still lacking, but sequence analysis (8) and site-selected mutagenesis have revealed that they share high structure similarity with LHCII, although they coordinate a smaller number of pigments (9,10).

CP29 is the largest member of the Lhc family, and it is characterized by a long N-terminal domain (~100 amino-acid residues), which contains a phosphorylation site (11). Phosphorylation takes place, for instance, under cold stress and is accompanied by a structural change of the protein (12). It has been shown that there is a strong correlation between the presence of phosphorylated CP29 and the resistance of plants against cold stress, thus leading to the suggestion that the phosphorylation is involved in protective mechanisms (13). However, details are lacking on both the structure and the structural changes.

Submitted November 18, 2008, and accepted for publication January 28, 2009.

*Correspondence: marcus.hemminga@wur.nl

Chl, chlorophyll; CP29, chlorophyll-*a*/*b*-binding protein 29 (a minor antenna complex of photosystem II); DM, n-Dodecyl β-D-maltoside; ESR, electron spin resonance; GHOST, condensation algorithm that filters and groups the solutions found in optimization runs; LDS, lithium dodecyl sulfate; Lhc, light-harvesting complex; LHCII, light-harvesting chlorophyll-*a*/*b*-binding protein of photosystem II; MTS-SL, (1-Oxyl-2,2,5,5-tetramethylpyrroline-3-methyl) methanethiosulfonate spin label; PS, photosystem.

Editor: David D. Thomas.

© 2009 by the Biophysical Society

0006-3495/09/05/3620/9 $2.00

doi: 10.1016/j.bpj.2009.01.038

CP29 belongs to the class of membrane proteins. In general, membrane proteins comprise almost one-third of the total amount of proteins in an organism or cell. However, progress in determining their structures has been slow. Therefore, membrane proteins offer an enormous challenge in structural biology, and there is an urgent need to develop and apply new biophysical methodologies that are able to generate detailed structural information. Among modern biophysical techniques, site-directed spin-labeling ESR appears to show the highest potential to further develop the field (14).

Recently, CP29 protein mutants reconstituted with plant pigments in detergent were selectively labeled at three positions in the N-terminal domain with a fluorescent dye TAMRA (6-carboxy-tetramethyl-rhodamine) and examined with picosecond fluorescence spectroscopy (15). The results indicated that the N-terminus is folded back on the hydrophobic part of the protein, and suggested the presence of some structural heterogeneity in the N-terminal part.

This work focuses on the structure and dynamics of the N-terminal domain of CP29 in detergent systems with and without pigments. Site-directed mutagenesis was used to produce 10 single-cysteine protein samples with cysteine positions equally distributed over the N-terminal domain. Following the approach of Stopar et al. (16), single-cysteine protein samples were labeled with nitroxide spin labels. The ESR data allowed us to determine the free rotational space, local dynamics, and polarity of the spin-labeled sites that reflect the pigment-binding properties of CP29 and to arrive at a topological model for the N-terminal domain.

MATERIALS AND METHODS

Construction and isolation of overexpressed CP29 apoprotein

Lhcb4.1 cDNA of *Arabidopsis thaliana* (*A. Thaliana*) (from *Arabidopsis* Biological Resource Center DNA Stock Center) was subcloned into a pT7-7 expression vector. The construct contains the sequence of the mature CP29 protein with an additional methionine at the N-terminus and a 6 His-tag at the C-terminus. Mutations were introduced using the Stratagene Quick Change Site Directed Mutagenesis Kit. First, the naturally occurring cysteine (position 108) was replaced by alanine. This mutant was also used to estimate the amount of nonspecific spin labeling. On this template, single-cysteine residues were introduced in the N-terminal part at various positions resulting in the following mutants: G4C, S15C, S33C, S40C, A56C, S65C, T81C, S90C, and S97C. The constructs were checked by DNA sequencing. The plasmids were amplified in the super competent *Escherichia coli* (*E. coli*) XL-1 Blue strain and the proteins overexpressed in the *E. coli* BL21 (*DE3*) strain. Inclusion bodies containing the CP29 apoprotein mutants were isolated as reported in (17,18) and stored in the presence of 10 mM dithiothreitol at −20°C.

Pigment isolation, labeling, and reconstitution of CP29-pigment complexes

Purified pigments were obtained from spinach. Concentrations of pigments were determined spectroscopically: Chls as described by Porra et al. (19) and carotenoids as described by Davies (20). Just before labeling, inclusion bodies containing CP29 apoprotein were freshly purified from dithiothreitol and dissociated in LDS reconstitution buffer (2% LDS, 12.5% sucrose, 20 mM Na_2HPO_4 pH 7.6). CP29 apoproteins were labeled at room temperature for 3 h with a five-times molar excess of the spin label MTS-SL (methanethiosulfonate from TRC, Toronto, Canada). Excess spin label was removed using affinity chromatography on a His-Trap column. Before storage at −20°C, the excess of imidazole and NaCl from the elution buffer were removed by dialysis against LDS reconstitution buffer. Samples of CP29 apoprotein to be measured in β-D-maltoside (DM) buffer (0.03% W/V + 10 mM Na_2HPO_4, pH 7.6) were prepared by using the detergent substitution procedure (21) followed by affinity chromatography on a His-Trap column to bring the apoprotein in DM buffer. Reconstitution and purification of protein-pigment complexes (holoproteins) were performed as reported in (22), but using a Chl *a*/*b* ratio of 5.5. Solutions of the spin-labeled CP29 samples were washed and concentrated in sucrose-free DM buffer just before the ESR measurements. Integrity of the holoprotein samples was checked by fluorescence excitation and emission measurements, showing the complete absence of free Chls and carotenoids in all preparations.

ESR measurements

All washed and concentrated spin-labeled CP29 preparations in DM buffer (final protein concentration between 0.07 mM and 0.2 mM) were transferred to 50 μl capillaries up to 1 cm height and placed in a standard 4-mm quartz ESR tube. Spectra were measured on an X-band Bruker Elexsys E-500 ESR system (Bruker, Rheinstetten, Germany) equipped with a super-high-Q cavity ER 4122SHQE in combination with a SuperX X-Band Microwave Bridge type ER 049X. Temperature was controlled with a quartz variable-temperature Dewar insert (Eurotherm, Leesburg, VA). Spectra were recorded at 10-mT scan widths with a microwave power of 5 mW at 6°C. To improve signal/noise, up to 100 scans were accumulated with a time constant of 20 ms, a modulation amplitude of 0.1 mT and a scan time of 82 s. Before analysis, spectra were corrected for the background signal of the buffer.

ESR spectral simulation, optimization, and solution condensation

The ESR spectra of spin-labeled CP29 samples were simulated with a multicomponent model as described previously (16,23). The spectral parameters $\{\vartheta, \varphi, \tau_c, W, p_A, prot\}$ of each component of the simulated spectra were simultaneously optimized with a multirun hybrid evolutionary algorithm (24,25). Multiple solutions, which were obtained from optimization, were then filtered and grouped into domains with a GHOST condensation approach (16,23,25,26).

The simulation model for the ESR spectra employs a fast motional averaging approximation to describe the local motion of the spin label (25). The dynamics of the spin probe gives rise to a motion in a cone (27), which can be described with three parameters: a maximum opening cone angle ϑ, a cone asymmetry angle φ, and an effective correlation time τ_c. The magnetic interaction tensors **g** and **A** are linearly corrected with a polarity parameter p_A. Furthermore, a proticity parameter *prot* is used that accounts for the effect of proton binding to the spin label on the **g** tensor (28). It was found that the relative error for parameter *prot* was quite large. Therefore this parameter is not used in our further discussion (23). When calculating the convolution of the magnetic field distribution and the basic line shape, two line width parameters, τ_c and W, are applied. A Lorentzian line is used in the motional narrowing approximation with a single effective rotational correlation time τ_c (27,29). The additional broadening of the spectral line arising from nonmotional effects is described by a constant W. This parameter arises from unresolved hydrogen superhyperfine interactions and contributions from paramagnetic impurities (e.g., oxygen), in addition to external magnetic field inhomogeneities, field modulation effects, and intermolecular spin-spin interactions if present and applicable.

To resolve coexisting motional patterns from the experimental ESR spectra, the simulated spectra were composed from four independent

spectral components defined by four sets of spectral parameters $\{\vartheta, \varphi, \tau_c, W, p_A, prot\}$ and four relative contributions following a previous approach (23). Typically, 20 runs of the population-based hybrid evolutionary optimization were used to produce 8000 (400 in each of 20 runs) solutions (spectral parameters and the weights of four spectral components) (25,26). The 200 best solutions were chosen (according to the quality of fit), and their four spectral components were separated into a pool of 800 parameter sets. Collected single-spectral components are processed further with GHOST condensation, which filtered and then grouped the spectral components into domains (25,26). Each domain in a GHOST plot can be seen as a "motional pattern" of the spin label that is related to its local motional properties. Such motional patterns reflect the restrictions of the spin label arising from the local protein structure, i.e., local interactions between the spin-label rotamers and neighboring amino-acid side chains and the motional limitations imposed by the protein backbone. In addition, the motional patterns reflect different dynamical regimes of the spin probe, which may additionally include: a), dynamics inherited from the whole protein motion, and b), protein backbone fluctuations (27). Also the spin label senses the accessibility of solvent molecules and adjacent acyl chain of the phospholipids in case it is in bilayer.

Filtering of the multiple solutions was done according to the fit quality of a particular solution and according to the density of the solution in the parameter space. The group recognition was done with a slicing method based on domain detection at several density levels (30). Visual analysis of the resulting GHOST plots, which present a combination of two parameters (φ and ϑ, τ_c and ϑ, p_A and ϑ), was used to revise the results of the automated group (motional patterns) recognition and to examine the distribution of the spectral characteristics within the groups. Candidate motional patterns were tested for their physical relevance by looking at the corresponding line shapes. Unusual line shapes resulting from abnormal combinations of parameters were omitted from further analysis. In this way the ESR experimental spectra are characterized in terms of multiple motional patterns, and the GHOST analysis provides the number of patterns, average parameters, and relative contribution of each pattern.

RESULTS

CP29 reconstitution

Together with the wild-type CP29 (WT-C108) nine cysteine-spin-labeled CP29 apoproteins (G4C/C108A, S15C/C108A, S33C/C108A, S40C/C108A, A56C/C108A, S65C/C108A, T81C/C108A, S90C/C108A, and S97C/C108A) were obtained and reconstituted with pigments in vitro. All pigment-protein complexes were obtained in their monomeric state as assessed by sucrose gradient ultracentrifugation. The absorption spectra of the holoprotein mutants are identical to that of the wild-type construct and resemble the spectrum of the native CP29 complex, similar as in previous studies (9,21,31). This indicates that the mutations do not influence the pigment binding.

ESR experiments

The ESR spectra of the reconstituted holoprotein complexes and of the apoproteins in detergent solution are shown in Fig. 1. In all cases the spectra have a multicomponent character. As can be seen, the absence of the pigments has only a small effect on the spectra corresponding to positions 15, 65, 81, and 90, and for all these cases the ESR spectra show a strong sharp three-line component of mobile spin labels. In contrast, for positions 33, 40, 56, 97, and 108, there

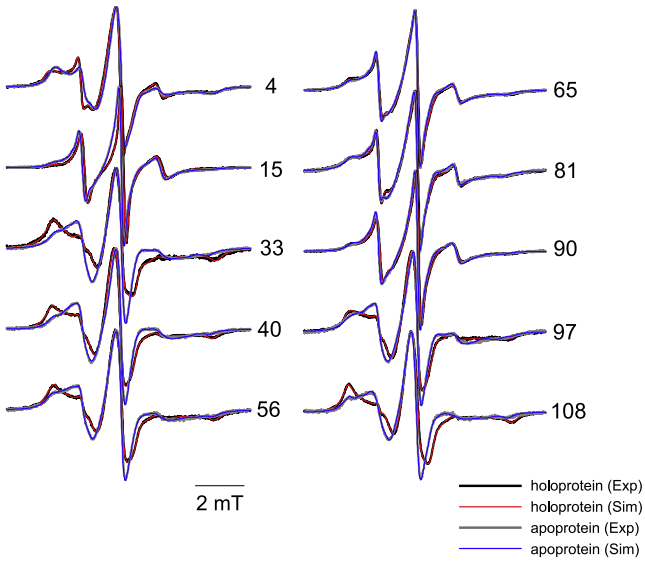

FIGURE 1 ESR spectra of MTS-SL spin-labeled CP29 protein samples at label positions 4, 15, 33, 40, 56, 65, 81, 90, 97, and 108 reconstituted in DM with (holoprotein, *black line*) and without (apoprotein, *gray line*) pigments. The total horizontal scan range is 10 mT. Spectral line heights are normalized to the same central line height (*left peak*). The simulated spectra are shown in red for holo- and blue for apoprotein samples.

is a relatively large spectral difference between the holo- and apoproteins. At these positions, the ESR spectrum has a typical immobile appearance, especially for the holoprotein in the presence of pigments. The ESR spectrum corresponding to position 4 shows a two-component spectrum with a strong immobile contribution. Close inspection of the ESR spectra corresponding to positions 4 and 15 reveals that there is a small increase of immobile component for the apoprotein.

To decompose the multicomponent ESR spectra, we used a multicomponent model of asymmetric motional restriction (16,23) and optimized the fitted spectra employing a multirun multisolution hybrid evolutionary method (25). The goodness of fit was chosen to be the reduced χ^2 function:

$$\chi^2 = \frac{1}{N}\sum_{i=1}^{N}\frac{\left(y_i^{exp} - y_i^{sim}\right)^2}{\sigma^2}, \qquad (1)$$

where y^{exp} and y^{sim} are the experimental and simulated data, respectively; σ is the standard deviation of the experimental points; and N is the number of spectral points (in our case $N = 1024$). For all 10 spin-labeled CP29 holo- and apoprotein samples, the quality of the simulated ESR spectra is good (see Fig. 1). For holoprotein spin labeled at positions 33, 56, 81, and 97 and apoprotein spin labeled at positions 4, 56, 81, and 108, the reduced χ^2 of the best-fit solutions is between 1.6 and 3. For the other samples, this is slightly higher, i.e., between 3 and 5. In general, χ^2 values below 5 can be considered to be very good.

The results from the simulations are summarized in so-called GHOST plots (such as a $\vartheta-\varphi$ GHOST shown for

positions 65 and 108 in Fig. 2). The GHOST methodology provides the motional patterns that characterize the spectrum, thus the GHOST plots provide the most significant and probable groups of solutions of spectral parameters. Each group corresponds to a particular motional pattern (e.g., mobile or immobile according to the rate of motion; restricted or unrestricted according to the extent of restrictions imposed by the local protein structure on free rotational space of the spin probe). The weight of the group represents the contribution of that particular component to the spectrum. For example, at position 65 (Fig. 2), the rotational space of the component with 14% contribution is completely open (ϑ and φ around $\pi/2$), a component with a contribution of 57% is half-closed (ϑ around $\pi/4$) and still symmetric (φ around $\pi/2$), and a component with a contribution of 16% is very closed (ϑ around $\pi/6$ and φ close to 0), as suggested by the distribution of the cone angles of the spin label ϑ and φ (both angles can vary between 0 and $\pi/2$). On the other hand, the rotational space for the spin label at position 108 of CP29 pigment-protein complex is very restricted as suggested by the major component with a contribution of 51% (ϑ around $\pi/6$ and φ close to 0) (Fig. 2). In most cases, the motional patterns in the GHOST plots (as shown in Fig. 2) are represented in the parameter space by concentrated groups of solutions. Contrary, in the case of spin-labeled apoprotein mutants 40 and 90, there appear continuous patterns, which reflect smooth transitions between the spectral parameters. This may indicate a transition between structural conformations, or could represent a distribution of a local structure around the mutated residue. The samples having spectra with a relatively low signal/noise turned out to be somewhat more problematic in terms of group recognition. Also the ESR spectra of mutants at positions 15 and 90 were more difficult to fit, and after group recognition, many spectral components were found distributed in the parameter space. Thus, after group recognition, the final solution appeared to contain several motional patterns with a low contribution (see Fig. 4). This means an additional complexity of the corresponding spectra and consequently of the spin-label motion at positions 15 and 90 relative to other spin-labeled positions. The four best-fitting spectral components in the simulated spectra (Fig. 1) are presented in the GHOST plots with colored triangles (Fig. 2). The size of a triangle is proportional to the contribution of the corresponding component in the spectrum.

For further analysis (i.e., a more convenient comparison of multiple data between different spin-label positions along the protein), the angles ϑ and φ are combined in a single parameter, Ω, which is defined as (23):

$$\Omega = \frac{\vartheta\varphi}{(\pi/2)^2}. \tag{2}$$

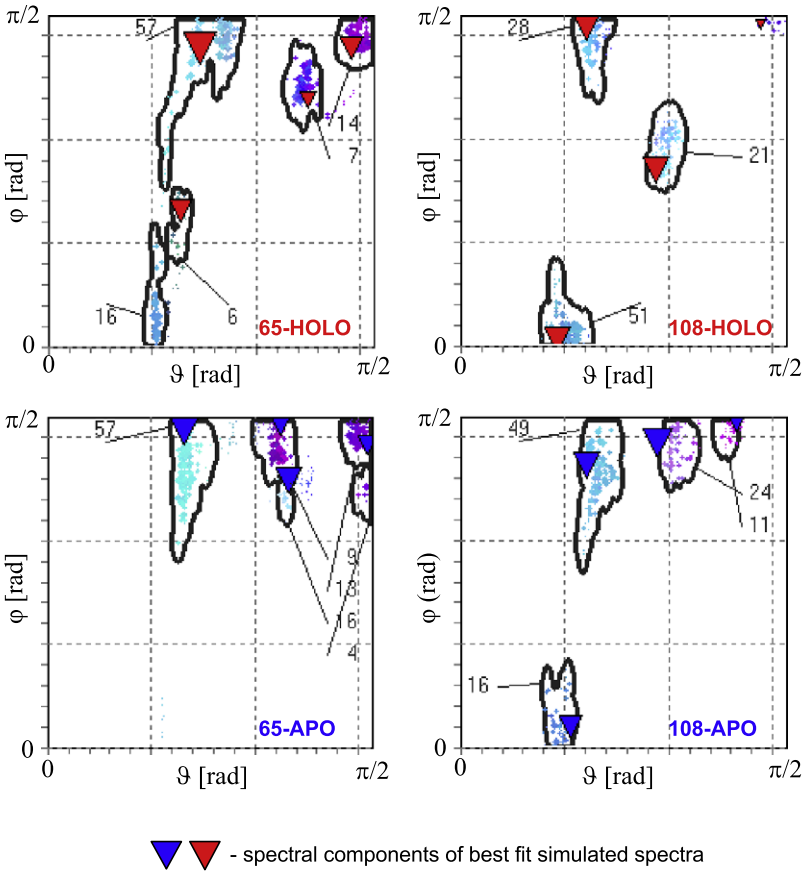

FIGURE 2 GHOST plots showing the optimized multiple solutions represented in a two-dimensional distribution of the angles ϑ and φ of MTS-SL spin-labeled CP29 protein samples at positions 65 and 108 reconstituted in DM with (*top*, holoprotein) and without (*bottom*, apoprotein) pigments. The components of each solution are represented with a point on the plot with a color, combined of red, green, and blue, which codes for the relative values of τ_c, W, and p_A in their definition intervals {0–3 ns}, {0–0.4 mT}, and {0.8–1.2}, respectively. The closed black lines on the plot surround domains of the solutions grouped into motional patterns. The contribution of each pattern is shown in percents. Additionally, the four spectral components of the best-fit solution are presented on the plot with red (*top*, holoprotein) and blue (*bottom*, apoprotein) triangles, whereby the area of each triangle is proportional to the relative contribution of the corresponding component in the simulated spectrum.

This parameter measures the space angle, i.e., the surface of the cone left for local spin-label wobbling (free rotational space) and is shown for all 10 spin-labeled CP29 holo- (Fig. 3 *A*) and apoprotein samples (Fig. 3 *B*). High values of Ω (between 0.7 and 1) correspond to nearly unrestricted motional patterns of the spin label (i.e., mobile spectral components), whereas low values (between 0 and 0.25) imply very high restrictions (i.e., immobile spectral components). In addition to the free rotational space Ω, the simulations provide the effective rotational correlation time τ_c (29) and the polarity correction p_A for the magnetic interaction tensors **g** and **A** of the spin label (16,28). These parameters are presented in Fig. 3, *A* and *B*, as well. To elucidate the effect of pigment removal on the ESR data, we carried out a comparison of the most important motional patterns (with a contribution of more than 25%), as shown in Fig. 3 *C*. Fig. 3 *D* compares the weighted averages of the motional patterns of the spin-labeled holo- and apoproteins. In general, it can be seen in Fig. 3 that high values of the free rotational space Ω correspond to high values of the effective rotational correlation time τ_c.

DISCUSSION

The central issue in our research is related to the following questions: 1), What is the conformation of the unusually 100-residues long N-terminal domain of CP29 protein (which is much longer than for all other members of the Lhc family)? 2), Where is this domain located with respect to the membrane-embedded transmembrane protein body? and 3), What is the role of the pigments in determining the structure and dynamics of the N-terminal domain? To address these questions, we compared CP29 holo- and apoprotein by using ESR of spin-labeled cysteine positions distributed over the N-terminal domain. In this respect, it should be noted that after reconstitution in the detergent DM, the pigments provide a correctly folded transmembrane body domain of the protein, which can be considered as the native state of the protein (21,32,33). The detergent that is used for the reconstitution of CP29 protein with the pigments provides a good membrane-mimicking environment for CP29: DM is not a very strong denaturing detergent providing a relatively compact protein-detergent complex (33). If the pigments are absent, the structure of CP29 protein is looser and it may be partly unfolded (33). For LHCII in DM, the spectroscopic properties are similar to those observed in the intact thylakoid membrane (34). Because LHCII and CP29 have a strong sequence homology in the transmembrane protein body (9), this indicates that the structure of CP29 in DM may also be similar to the in vivo structure. Thus, the holo- and apo-states of CP29 provide a good

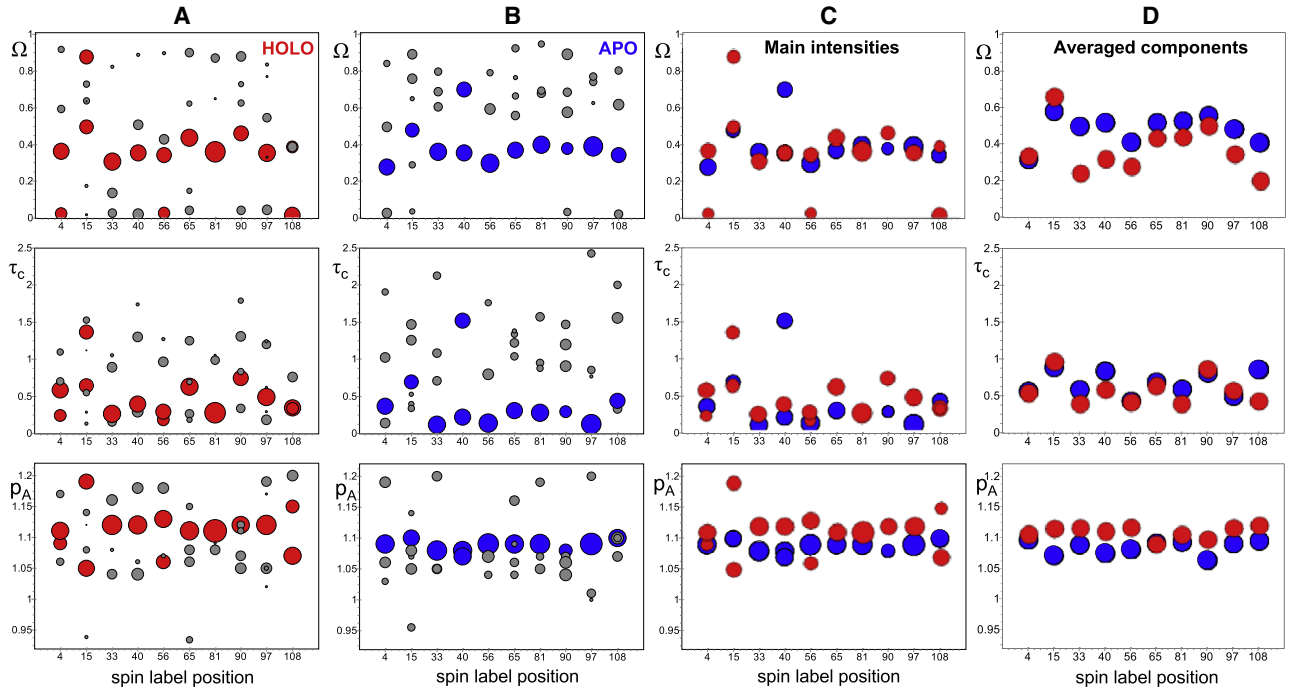

FIGURE 3 ESR data of MTS-SL spin-labeled CP29 protein samples reconstituted in DM with (*A*) (holoprotein, *red circles*) and without (*B*) (apoprotein, *blue circles*) pigments. Less-pronounced motional patterns with a contribution below 25% are represented by gray circles. The horizontal axis indicates the spin-label position, the vertical axes give Ω, τ_c, and p_A. High values of Ω (between 0.7 and 1) correspond to (nearly) unrestricted motional patterns of the spin label (i.e., mobile spectral components), whereas low values (between 0 and 0.25) imply very high restrictions (i.e., immobile spectral components). (*C*) Comparison of the most important motional patterns (with a contribution of more than 25%) of spin-labeled CP29 protein samples with (holoprotein, *red circles*) and without pigments (apoprotein, *blue circles*). (*D*) Weighted averages of the motional patterns of spin-labeled CP29 protein samples with (holoprotein, *red circles*) and without pigments (apoprotein, *blue circles*). The area of the circles in *A*, *B*, and *C* is proportional to the relative contribution of the motional patterns to the multiple solution.

starting point for a comparative spin-label ESR study addressing the questions given above.

From a qualitative analysis of the ESR spectra (Fig. 1), it follows that positions 33, 40, 56, 97, and 108 are located in protein domains that are strongly affected by pigment reconstitution of the CP29 complex. Positions 97 and 108 are located in the transmembrane protein body that contains the pigments (11). It is evident that these positions will be affected by the pigment reconstitution, bringing the protein from a relatively loose and partly unfolded structure without pigments into a native folded structure with pigments. Interestingly, positions 33, 40, and 56 follow the same trend. This indicates that this protein domain is located adjacent to the transmembrane protein body. Positions 65, 81, and 90 show a sharp mobile component indicating a relatively high degree of motion. Moreover, these positions are not affected by pigment reconstitution, suggesting that they are located far from the transmembrane region in a loop extending out from the stromal surface of the protein (11). Also positions 4 and 15 at the N-terminal end are just slightly affected by pigment reconstitution. Position 4 displays a clear two-component characteristic of a sharp mobile and a broad immobile component. Contrary, position 15 can be characterized only by a sharp mobile component, and the broad immobile component is almost absent. This indicates that the spin label at position 4 is more restricted in its motion than the one at position 15. This finding is remarkable, because position 4 is close to the N-terminal end, where one would expect a large degree of motion due to fraying of the terminal amino-acid residues. The ESR line shapes at positions 15, 65, 81, and 90 are roughly similar to each other.

To further analyze the multicomponent ESR spectra, we carried out a spectral decomposition based on a multicomponent model of asymmetric motional restriction (16,23), followed by a multirun, multisolution hybrid evolutionary approach (25). The multicomponent model turned out to be robust enough to cover many different combinations of coexisting local motional patterns. The multisolution feature of the simulations provides the capability of determining the actual number of the spectral components related to spin-probe motional patterns, the spectral parameters and the contribution of each component, without setting the number of the spectral components in advance. Due to practical considerations, we limited the maximum number of spectral components to four.

The main general advantages of our multiple-solution algorithm are: 1), determination of multiple components (motional patterns), because a single solution characterization may not be capable of revealing all components; 2), revealing a transition between spectral parameters, which could be very useful in the case of multiple protein conformations; 3), detecting defects in the line shape. Concerning line shape defects, a spectral component may arise in the optimization to simulate a particular feature of the line shape to improve the fit. In such a case, checking of the parameter space via GHOST plots (such as shown in Fig. 2) in combination with the line-shape analysis helps to clarify the characterization results and to remove meaningless components, if needed (23,25). Also, the appearance of low-quality fits and an unusual distribution of the spectral parameters in the parameter space may indicate artifacts in the spectra. In most cases, we found high-quality fit solutions and well-defined two-dimensional GHOST patterns, indicating that the ESR spectra do not have artifacts and that the group recognition was carried out in a correct way.

As can been seen in Fig. 3, *A* and *B*, the GHOST analysis results in a number of motional patterns. There are several factors that can contribute to a multicomponent character: 1), differences in local structure around the spin label at the binding site; 2), various rotamers of the side chain of the spin label and interactions between certain rotamers with the local environment; 3), sample heterogeneity on the level of the micelles in which CP29 protein is incorporated, for example arising from differences in protein-to-detergent ratios and micellar sizes; and 4), nonspecific labeling. To estimate the amount of nonspecific labeling, we produced a mutant of wild-type CP29, in which the cysteine at position 108 is replaced by an alanine. Spin labeling of this mutant shows that the amount of nonspecific labeling is 5%. As can be seen in Fig. 3 *A* even by discarding motional patterns with small contributions ($<$10–20%), there is more than one component left in a majority of the cases.

Because the free rotational space Ω is very sensitive to the local environment of the spin-label side chain (adjacent protein domains and/or solvent molecules), there are two different ways to handle multiple motional patterns:

1. Assign the motional patterns to one or two protein conformations and further use this result to interpret the effect of pigment binding on the conformation of the protein and locations of the pigments in the protein. In this case, we select the components with the highest intensity (above 25%) in the GHOST analysis (Fig. 3 *C*). The other motional patterns are then assigned to sample heterogeneities and minor structural components. Two or more components may manifest similarities, consistent changes of the model parameters, and thus can be considered to be parts of a single major motional pattern. Such a pattern (prolonged in parameter space) with an evident transition of the model parameters then most likely represents the transition between conformational states. This enables an analysis of the results in terms of different protein conformations.
2. As we will concentrate on the effect of pigment binding of CP29 protein, we do not need to assign the various motional patterns, but we can focus on the differences in the results with and without pigments. Therefore another approach is to take the weighted average of all patterns (Fig. 3 *D*). When comparing the averaged data for the protein with and without pigment, the difference will be dominated by the effect of pigment binding.

In comparing the Ω values for the holo- and apoprotein in Fig. 3, *A* and *B*, it can be seen that for almost all spin-label positions the range of values increases from low values to higher values. This is especially true for the motional patterns with $\Omega \approx 0$ in Fig. 3 *A*, in which the spin-label motion is highly restricted. These motional patterns are almost gone in Fig. 3 *B*. In turn, in Fig. 3 *B* a larger range of motional patterns is observed for Ω values from 0.6 to 1.0, indicating local conformations with less-restricted spin-label motion. Because this effect is found throughout the whole N-terminal domain, it is assigned to partly unfolding of the protein on going from the holo- to the apo-state. As can be seen in the intensity-filtered data in Fig. 3 *C*, at several positions (4, 15, 40, 56, and 108) two values for Ω, τ_c, and p_A can be identified. These positions appear to be spread over the entire sequence of the N-terminal domain of CP29 protein. This effect is also related to a relatively loose and partly unfolded state of the apoprotein, as discussed above. However, no consistent pattern exists between the various values for Ω, complicating a detailed analysis of the data in terms of different conformations of the N-terminal protein domain. Although there appears to be a wealth of information in Fig. 3, *A* and *B*, a full assignment of motional patterns is not possible without additional knowledge about the N-terminal domain and without having more amino-acid residues systematically replaced in a certain protein domain.

This difficulty does not exist by taking the weighted average of all motional patterns (Fig. 3 *D*). These data represent the general trend, but details about the various components are lost. In Fig. 3 *D*, apart from information about the average free rotational space Ω, information is available about the average effective rotational correlation time τ_c and local polarity p_A of the spin label attached to the protein. In Fig. 3 *D*, it can be seen that in all cases (except for positions 4 and 15) the values for Ω for the pigment-free CP29 protein are above the values for the reconstituted protein. This indicates that the N-terminal part of the pigment-free apoprotein has a relatively loose and flexible structure in which the available space for the spin label is expected to be less restricted. Based on the polarity effect shown in Fig. 3 *D* (a high value for p_A reflects an increased local polarity (25)), we can conclude that overall the spin-labeled sites in the apoprotein are more in an apolar environment as compared to the holoprotein. This could reflect an enhanced exposure to the acyl chains of the solubilizing detergent molecules, probably due to the relatively loose and partly unfolded state of the apoprotein.

The trend in the free rotational space Ω, as shown in Fig. 3 *D*, closely follows the qualitative interpretation of the ESR spectra in Fig. 1, indicating that the loop positions 65, 81, and 90 are only slightly affected by the pigment binding to CP29. Also the observed differences between the holo- and apo-state of the protein on positions 33, 40, 56, 97, and 108 are consistent with the analysis of Fig. 1. In the N-terminal domain, position 4 is slightly affected by the absence of pigment; however, its value for Ω is similar to the values for the positions in the more structured domains. This is remarkable for an N-terminal end position and could indicate a local structure that limits the free rotational space of the spin label. Alternatively, this N-terminus could interact with the transmembrane protein body, which is in agreement with recent fluorescence experiments with the fluorescent dye TAMRA (6-carboxy-tetramethyl-rhodamine) covalently attached to a cysteine at position 4 (15). In contrast, position 15 does not show a strong effect to pigment removal, but its value for Ω is at a high level, indicating rather unrestricted spin-label motion at a location probably relatively far from the transmembrane protein body.

Summarizing model

CP29 has a strong sequential homology with LHCII, the major difference being an N-terminal insert from amino-acid residue 56 to 98 (9). Also light-spectroscopic experiments have revealed a high degree of structural and functional similarity between CP29 and LHCII and demonstrate an unequivocally high similarity for the transmembrane protein bodies (22,35–38). Because of this strong sequence homology and spectroscopic similarities, we took the crystal structure of LHCII from spinach (7) as a starting point for constructing a model for CP29 (Fig. 4). In this figure, the extra N-terminal insert is shown as a red loop extruding from the main protein body. The amino-acid residues 97 and 108 that were used for spin labeling are located in the transmembrane protein body of the protein. Position 108 is situated on the putative transmembrane helix B of the protein, close to the center plane of the protein; position 97 is at the end of this helix, close to the stromal surface of the protein. These locations are consistent with the relatively strong difference between holo- and apoprotein and the relatively low values of Ω that are indicative for a restricted spin-label motion (Fig. 3). Positions 65, 81, and 90 are located in the extra N-terminal loop that is proposed to extend out of the protein in the stromal space, because for these sites, the label has a large degree of freedom and is not influenced by pigment binding. This loop also contains a phosphorylation site at Thr81. This finding suggests that the flexibility of this loop could play a role in presumed regulatory functions of the phosphorylation.

Positions 33, 40, and 56 show far less rotational freedom, and moreover, the corresponding ESR spectra are substantially affected by pigment reconstitution, indicating that the domain in which they are located should be close to the transmembrane protein body. Their relatively low values for Ω are similar to the values found for positions 97 and 108 (Fig. 3). This observation is consistent with the crystal structure of LHCII, in which these positions are located in a folded protein domain at the stromal side of the protein (7) (Fig. 4). The next labeled position toward the N-terminal end, position 15, shows a high value for Ω suggesting rather unrestricted spin-label motion. This indicates that this

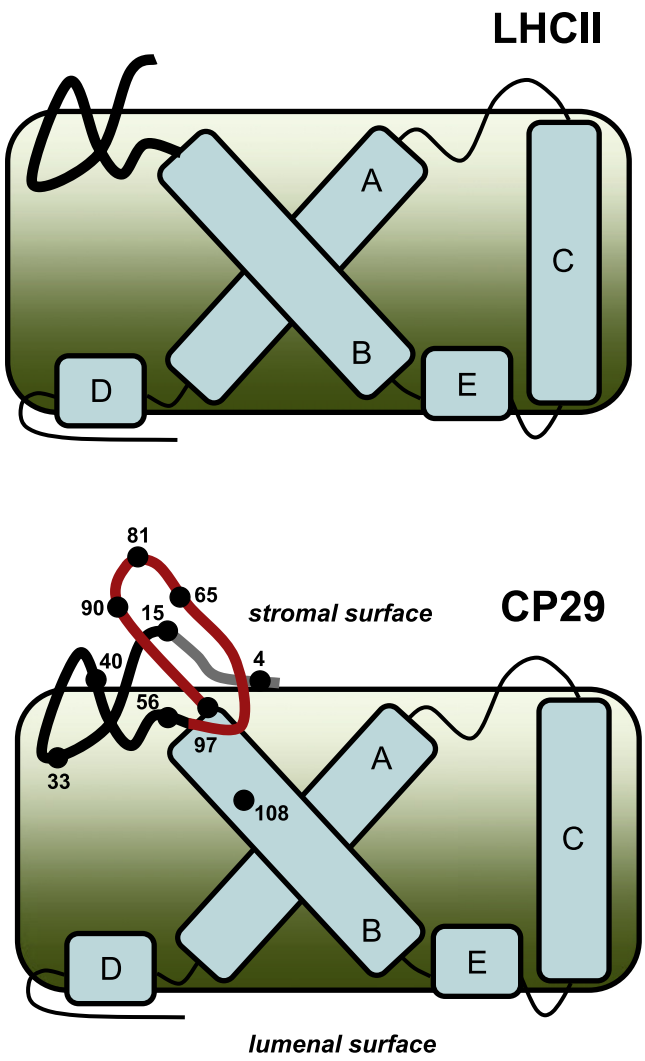

FIGURE 4 Schematic structural model of CP29 based on the crystal structure of LHCII from spinach (7) (Protein Data Bank ID: 1RWT). The main helical structures (*A–E*) of the transmembrane protein body are shown in light blue. The extra N-terminal insert of CP29 (as compared to LHCII) is shown as a red loop extruding from the main transmembrane protein body. The N-terminus from amino-acid residue 1–14 is indicated in gray, as this part of the structure is not resolved in the crystal structure of LHCII. The numbers refer to the labeled positions (*black dots*).

protein domain is in a flexible state. This is in agreement with the finding that the structure of the N-terminal amino-acid residues 1 to 14 is not resolved in the crystal structure of LHCII. Finally, position 4 at the N-terminal end displays clear two-component characteristics of a broad immobile component in combination with a sharp mobile one (Figs. 1 and 3 *C*). It is slightly affected by the absence of pigments; however, its value for Ω (Fig. 3 *D*) is similar to the values for the positions in the more motionally restricted domains (i.e., position 97). This suggests that the N-terminus interacts with the transmembrane protein body probably by folding back to it; however, without being strongly affected by the holo- or apo-state of the protein. This topology is in agreement with recent fluorescence experiments with the fluorescent dye TAMRA (6-carboxy-tetramethyl-rhodamine) covalently attached to a cysteine at position 4 that indicate that in ~80% of the cases the N-terminus is folded back on the hydrophobic core (15). Next to position 4, there are two phenylalanine residues. It could be hypothesized that this domain interacts with the hydrophobic amino-acid residues that can be found in a groove on the stromal side of the transmembrane protein body.

Until so far, we have limited ourselves to analyze the ESR spectra of singly spin-labeled CP29 protein mutants. The main difficulty that we encountered was the limited number of available single-cysteine mutants, but this problem can be tackled by a high-throughput approach. In addition, a double-labeling approach can be applied that provides distances between spin labels placed in various domains of the protein, in a similar way as has been carried out for the major light-harvesting Chl *a*/*b* protein (LHCIIb) (39). Therefore, site-directed spin-labeling ESR spectroscopy is an attractive and powerful way to study the conformation and topology of the protein domains in CP29.

This work was supported by the Stichting voor Fundamenteel Onderzoek der Materie (FOM), which is financially supported by the Nederlandse Organisatie voor Wetenschappelijk Onderzoek (NWO). We thank Emilie Wientjes for making seminal contributions to this work.

REFERENCES

1. Nelson, N., and C. F. Yocum. 2006. Structure and function of photosystems I and II. *Annu. Rev. Plant Biol.* 57:521–565.
2. Jansson, S. 1999. A guide to the Lhc genes and their relatives in Arabidopsis. *Trends Plant Sci.* 4:236–240.
3. Caffarri, S., R. Croce, L. Cattivelli, and R. Bassi. 2004. A look within LHCII: differential analysis of the Lhcb1–3 complexes building the major trimeric antenna complex of higher-plant photosynthesis. *Biochemistry.* 43:9467–9476.
4. Dekker, J. P., and E. J. Boekema. 2005. Supramolecular organization of thylakoid membrane proteins in green plants. *Biochim. Biophys. Acta.* 1706:12–39.
5. Avenson, T. J., T. K. Ahn, D. Zigmantas, K. K. Niyogi, Z. Li, et al. 2008. Zeaxanthin radical cation formation in minor light-harvesting complexes of higher plant antenna. *J. Biol. Chem.* 283:3550–3558.
6. Ahn, T. K., T. J. Avenson, M. Ballottari, Y.-C. Cheng, K. K. Niyogi, et al. 2008. Architecture of a charge-transfer state regulating light harvesting in a plant antenna protein. *Science.* 320:794–797.
7. Liu, Z., H. Yan, K. Wang, T. Kuang, J. Zhang, et al. 2004. Crystal structure of spinach major light-harvesting complex at 2.72 Å resolution. *Nature.* 428:287–292.
8. Green, B. R., and D. G. Durnford. 1996. The chlorophyll-carotenoid proteins of oxygenic photosynthesis. *Annu. Rev. Plant Physiol. Plant Mol. Biol.* 47:685–714.
9. Bassi, R., R. Croce, D. Cugini, and D. Sandonà. 1999. Mutational analysis of a higher plant antenna protein provides identification of chromophores bound into multiple sites. *Proc. Natl. Acad. Sci. USA.* 96:10056–10061.
10. Sandonà, D., R. Croce, A. Pagano, M. Crimi, and R. Bassi. 1998. Higher plants light harvesting proteins. Structure and function as revealed by mutation analysis of either protein or chromophore moieties. *Biochim. Biophys. Acta.* 1365:207–214.
11. Testi, M. G., R. Croce, P. P.-D. Laureto, and R. Bassi. 1996. A CK2 site is reversibly phosphorylated in the photosystem II subunit CP29. *FEBS Lett.* 399:245–250.

12. Croce, R., J. Breton, and R. Bassi. 1996. Conformational changes induced by phosphorylation in the CP29 subunit of Photosystem II. *Biochemistry*. 35:11142–11148.

13. Mauro, S., P. Dainese, R. Lannoye, and R. Bassi. 1997. Cold-resistant and cold-sensitive maize lines differ in the phosphorylation of the photosystem II subunit, CP29. *Plant Physiol*. 115:171–180.

14. Hemminga M. A., and L. J. Berliner, editors. 2007. ESR spectroscopy in membrane biophysics. Springer, New York.

15. Van Oort, B., S. Murali, E. Wientjes, R. B. M. Koehorst, R. B. Spruijt, et al. 2009. Ultrafast resonance energy transfer from a site-specifically attached fluorescent chromophore reveals the folding of the N-terminal domain of CP29. *Chem. Phys*. 357:113–119.

16. Stopar, D., J. Štrancar, R. B. Spruijt, and M. A. Hemminga. 2005. Exploring the local conformational space of a membrane protein by site-directed spin labeling. *J. Chem. Inf. Model*. 45:1621–1627.

17. Nagai, K., and H. C. Thøgersen. 1987. Synthesis and sequence-specific proteolysis of hybrid proteins produced in Escherichia coli. *Methods Enzymol*. 153:461–481.

18. Paulsen, H., U. Rümler, and W. Rüdiger. 1990. Reconstitution of pigment-containing complexes from light-harvesting chlorophyll a/b-binding protein overexpressed inEscherichia coli. *Planta*. 181:204–211.

19. Porra, R. J., W. A. Thompson, and P. E. Kriedemann. 1989. Determination of accurate extinction coefficients and simultaneous equations for assaying chlorophylls a and b extracted with four different solvents: verification of the concentration of chlorophyll standards by atomic absorption spectroscopy. *Biochim. Biophys. Acta*. 975:384–394.

20. Davies, B. 1965. Analysis of carotenoid pigments. *In* Chemistry and Biochemistry of Plant Pigments. T. W. Goodwin, editor. Academy Press, New York. 489–532.

21. Giuffra, E., D. Cugini, R. Croce, and R. Bassi. 1996. Reconstitution and pigment-binding properties of recombinant CP29. *Eur. J. Biochem*. 238:112–120.

22. Croce, R., M. G. Muller, S. Caffarri, R. Bassi, and A. R. Holzwarth. 2003. Energy transfer pathways in the minor antenna complex CP29 of photosystem II: a femtosecond study of carotenoid to chlorophyll transfer on mutant and WT complexes. *Biophys. J*. 84:2517–2532.

23. Stopar, D., J. Štrancar, R. B. Spruijt, and M. A. Hemminga. 2006. Motional restrictions of membrane proteins: A site-directed spin labeling study. *Biophys. J*. 91:3341–3348.

24. Filipič, B., and J. Štrancar. 2001. Tuning EPR spectral parameters with a genetic algorithm. *Appl. Soft Comput*. 1:83–90.

25. Štrancar, J., T. Koklič, Z. Arsov, B. Filipič, D. Stopar, et al. 2005. Spin label EPR-based characterization of biosystem complexity. *J. Chem. Inf. Model*. 45:394–406.

26. Kavalenka, A. A., B. Filipič, M. A. Hemminga, and J. Štrancar. 2005. Speeding up a genetic algorithm for EPR-based spin label characterization of biosystem complexity. *J. Chem. Inf. Model*. 45:1628–1635.

27. Columbus, L., and W. L. Hubbell. 2004. Mapping backbone dynamics in solution with site-directed spin labeling: GCN4–58 bZip free and bound to DNA. *Biochemistry*. 43:7273–7287.

28. Steinhoff, H. J., A. Savitsky, C. Wegener, M. Pfeiffer, M. Plato, et al. 2000. High-field EPR studies of the structure and conformational changes of site directed spin labeled bacteriorhodopsin. *Biochim. Biophys. Acta*. 1457:253–262.

29. Štrancar, J., M. Šentjurc, and M. Schara. 2000. Fast and accurate characterization of biological membranes by EPR spectral simulations of nitroxides. *J. Magn. Reson*. 142:254–265.

30. Štrancar, J., T. Koklič, and Z. Arsov. 2003. Soft picture of lateral heterogeneity in biomembranes. *J. Membr. Biol*. 196:135–146.

31. Caffarri, S., F. Passarini, R. Bassi, and R. Croce. 2007. A specific binding site for neoxanthin in the monomeric antenna proteins CP26 and CP29 of Photosystem II. *FEBS Lett*. 581:4704–4710.

32. Paulsen, H., B. Finkenzeller, and N. Kühlein. 1993. Pigments induce folding of light-harvesting chlorophyll *a*/*b*-binding protein. *Eur. J. Biochem*. 215:809–816.

33. Horn, R., G. Grundmann, and H. Paulsen. 2007. Consecutive binding of chlorophylls *a* and *b* during the assembly *in vitro* of light-harvesting chlorophyll-*a*/*b* protein (LHCIIb). *J. Mol. Biol*. 366:1045–1054.

34. Hemelrijk, P. W., S. L. S. Kwa, R. van Grondelle, and J. P. Dekker. 1992. Spectroscopic properties of LHC-II, the main light-harvesting chlorophyll a/b protein complex from chloroplast membranes. *Biochim. Biophys. Acta*. 1098:159–166.

35. Gradinaru, C. C., I. H. M. van Stokkum, A. A. Pascal, R. van Grondelle, and H. van Amerongen. 2000. Identifying the pathways of energy transfer between carotenoids and chlorophylls in LHCII and CP29. A multicolor, femtosecond pump-probe study. *J. Phys. Chem. B*. 104:9330–9342.

36. Pascal, A., C. Gradinaru, U. Wacker, E. Peterman, F. Calkoen, et al. 1999. Spectroscopic characterization of the spinach Lhcb4 protein (CP29), a minor light-harvesting complex of photosystem II. *Eur. J. Biochem*. 262:817–823.

37. Mozzo, M., F. Passarini, R. Bassi, H. van Amerongen, and R. Croce. 2008. Photoprotection in higher plants: The putative quenching site is conserved in all outer light-harvesting complexes of photosystem II. *Biochim. Biophys. Acta*. 1777:1263–1267.

38. Mozzo, M., L. Dall'Osto, R. Hienerwadel, R. Bassi, and R. Croce. 2008. Photoprotection in the antenna complexes of photosystem II: role of individual xanthophylls in chlorophyll triplet quenching. *J. Biol. Chem*. 283:6184–6192.

39. Jeschke, G., A. Bender, T. Schweikardt, G. Panek, H. Decker, et al. 2005. Localization of the N-terminal domain in light-harvesting chlorophyll a/b protein by EPR measurements. *J. Biol. Chem*. 280:18623–18630.